

©(2007) Society of Photo-Optical Instrumentation Engineers (SPIE). One print or electronic copy may be made for personal use only. Systematic reproduction and distribution, duplication of any material in this paper for a fee or for commercial purposes, or modification of the content of the paper are prohibited.

Chai, Jyh Wen, Jing Wang, and Chein-I. Chang. "Mixed Principal-Component-Analysis/Independent-Component-Analysis Transform for Hyperspectral Image Analysis." *Optical Engineering* 46, no. 7 (July 2007): 077006. <https://doi.org/10.1117/1.2759225>.

<https://doi.org/10.1117/1.2759225>

Access to this work was provided by the University of Maryland, Baltimore County (UMBC) ScholarWorks@UMBC digital repository on the Maryland Shared Open Access (MD-SOAR) platform.

Please provide feedback

Please support the ScholarWorks@UMBC repository by emailing scholarworks-group@umbc.edu and telling us what having access to this work means to you and why it's important to you. Thank you.

Mixed principal-component-analysis/independent-component-analysis transform for hyperspectral image analysis

Jyh Wen Chai

Taichung Veterans General Hospital
Department of Radiology
Taichung, Taiwan
and

China Medical University
College of Medicine
Department of Radiology
Taichung

and
National Yang-Ming University
School of Medicine
Taipei, Taiwan

Jing Wang

University of Maryland
Baltimore County
Department of Computer Science
and Electrical Engineering
Remote Sensing Signal
and Image Processing Laboratory
Baltimore, Maryland 21250

Chein-I Chang, FELLOW SPIE

University of Maryland
Baltimore County
Department of Computer Science
and Electrical Engineering
Remote Sensing Signal
and Image Processing Laboratory
Baltimore, Maryland 21250
and
National Chung Hsing University
Department of Electrical Engineering
Environmental Restoration
and Disaster Reduction Research Center
Taichung, Taiwan

Abstract. Principal components analysis (PCA) and independent-component analysis (ICA) are widely used transforms to perform various tasks. Mixing both transforms has not been investigated. This paper develops a new transform, called the mixed PCA/ICA transform, which combines m principal components (PCs) produced by PCA and n independent components (ICs) generated by ICA to form a new set of $m+n$ mixed components to be used for hyperspectral image analysis. Four problems need to be addressed. One is to determine the total number of components, p , needed to be generated for the mixed (m, n) -PCA/ICA transform. The second is how to combine the PCA and ICA in a single transform. Since the ICA does not prioritize its generated ICs in the same way that the PCs are ranked by the PCA using data variances, how to generate an appropriate set of n ICs becomes a third problem. Finally, the fourth problem is to decompress the compressed data based on the mixed PCA/ICA components if there is a need to reconstruct the original data. This paper solves these four problems and further conducts experiments to demonstrate the utility of the mixed PCA/ICA transform in sub-pixel detection and mixed pixel classification and quantification. © 2007 Society of Photo-Optical Instrumentation Engineers. [DOI: 10.1117/1.2759225]

Subject terms: principal-component analysis (PCA); independent-component analysis (ICA); mixed PCA/ICA transform; virtual dimensionality (VD).

Paper 060567RR received Jul. 17, 2006; revised manuscript received Jan. 28, 2007; accepted for publication Jan. 29, 2007; published online Jul. 27, 2007. This paper is a revision of a paper presented at the SPIE conference on Chemical and Biological Standoff Detection III, Oct. 2005, Boston, Mass. The paper presented there appears (unrefereed) in SPIE Proceedings Vol. 5995.

1 Introduction

With the recent advent of imaging spectrometers, hyperspectral imagery can be now acquired and collected in hundreds of contiguous spectral bands (channels). Due to such highly correlated data and enormous data volumes, hyperspectral data compression has become increasingly important in data processing and analysis, particularly onboard processing.

In general, a hyperspectral image can be considered as an image cube with the third dimension specified by spectral bands. Many compression algorithms developed for hyperspectral image compression have been directly derived from compression algorithms for traditional 2-D still im-

ages or 3-D video images. The two most widely used such algorithms are JPEG2000¹⁻³ and 3-D set partitioning in a hierarchical tree (SPIHT).^{4,5} Unfortunately, it has been shown that such a direct application to hyperspectral imagery does not take full advantage of hyperspectral information provided by hundreds of bands, which seems more crucial than spatial information.⁶ On the other hand, because the spectral information in multispectral imagery may not be as important as that in hyperspectral imagery due to the low spectral resolution produced by only tens of discrete spectral bands, spectral compression has not received as much attention as spatial compression has.

The difference between multispectral and hyperspectral imagery lies in two key factors. One is the significantly improved spectral resolution for hyperspectral imagery, which has more than 10 times better spectral resolution that

multispectral image does. The other is its utility in applications where the multispectral imagery has been mainly focused on spatial-domain analysis for land cover/use classification in agriculture, ecology, geology, environmental monitoring, geographical information systems (GISs), etc., whereas hyperspectral imagery has been primarily developed for subpixel detection and mixed pixel analysis of subtle materials such as anomalies, small targets, and rare substances with very limited spatial extent. Under these circumstances, hyperspectral image analysts intend to perform data processing based on spectral characteristics rather than spatial properties. This implies that the spectral information is more important than the spatial information when it comes to hyperspectral data exploitation, specifically, hyperspectral data compression. As a consequence, blind use of 3-D compression techniques without extra care may result in loss of significant information in terms of spectral characterization. In order to mitigate this dilemma, a common approach is to perform spectral compression using the principal components analysis (PCA)⁷ followed by spatial compression.

However, two key issues arise from the use of PCA and spatial compression. The first issue is how many principal components (PCs) need to be retained for information preservation. The second issue is the limitation of information preserved by the PCA, which can only preserve information characterized by second-order statistics. As a result of their high spectral resolution, hyperspectral data generally reveal subtle information that cannot be uncovered by second-order statistics—for instance, anomalies. So, using only PCA-spectral based hyperspectral data compression may miss crucial information, which can be captured by high-order statistics in hyperspectral imagery. A recent study⁸ has shown that the independent components analysis (ICA)⁹ was very effective in automatic target recognition for this purpose. However, if only ICA-based hyperspectral data compression is performed, the information of the first two second-order statistics may thereby be lost through the preprocessing (sphering) implemented by the ICA. Accordingly, a more appropriate and effective spectral-based compression will be one that can combine advantages of both transforms so that the information characterized by statistics of second and higher orders can be retained and preserved. Unfortunately, this is more easily said than done, and thus far, no such work has been reported.

In addition to the same issue arising in the PCA-based spectral compression, namely, how many components have to be retained, another major problem arises: that the ICA does not prioritize the independent components (ICs) it generates, due to its use of random initial projection vectors. Furthermore, how to combine these two transforms and reconstruct from mixed PCs and ICs is another challenging issue, because they cannot be simply concatenated without taking extra caution.

This paper presents a new approach, called the mixed PCA/ICA transform, which mixes the PCA and ICA transforms to perform spectral compression. The rationale of our proposed transform is the following. It is often the case that the background of a hyperspectral image accounts for most image pixels, while the target pixels of interest only constitute a small pool of sample vectors compared to the entire image. In view of this, image background information is

generally characterized by second-order statistics, as opposed to target information, which can be captured by high-order statistics. However, this does not necessarily imply that the image background can be *completely* characterized by second-order statistics. On some occasions, the background does contain information of interest, which may be also described by high-order statistics. In this case, such information may not be preserved in major PCs, but rather in minor components. On the other hand, the ICA is developed to capture information specified by statistical independence in ICs. In doing so, it performs sphering as a preprocessing to remove second-order statistics so that they will not affect its generated ICs. Therefore, in order to retain information characterized by second-order statistics in PCs that may include mostly background information—as well as the target information, which can be captured by high-order statistics such as statistical independence in ICs—combining the PCs and ICs seems to provide a better way.

This, however, does not imply that the PCA cannot extract small objects or the ICA cannot extract background information. Indeed, despite the fact that the PCA ranks the components in terms of the second-order statistics (i.e., variances), those small objects that appear in the minor components can be still extracted as long as a sufficient number of components are included. Similarly, despite the fact that FastICA does not rank the ICs in terms of high-order statistics, FastICA can still extract background information in its ICs as long as the background (objects or materials) is not Gaussian-distributed. So, the issue is how to determine enough components to perform what it is required in various applications. This is exactly the goal of the proposed mixed PCA/ICA transform.

The first and foremost task for our transform is to determine the number of components, p , to generate. This same problem also arises in the PCA and ICA transforms, but has not been solved in the past. Interestingly, a new concept, called *virtual dimensionality* (VD), recently developed in Refs. 10 and 11, has been shown to be effective in dimensionality reduction.^{8,12} The utility of the VD in various application was also investigated and further explored.^{13,14} It turns out that the VD can be used for our purpose to estimate p . Using the VD-estimated value to determine the number of components, the mixed PCA/ICA spectral compression includes the PCA-based spectral compression and the ICA-based spectral compression as special cases. In other words, the mixed PCA/ICA spectral compression can be described more specifically as mixed (m,n) -PCA/ICA, which mixes m PCs and n ICs for spectral compression with $m+n=p$, where p is estimated by the VD. If $m=p$ and $n=0$, then mixed $(p,0)$ -PCA/ICA spectral compression is reduced to PCA-based spectral compression. On the other hand, if $m=0$ and $n=p$, then mixed $(0,p)$ -PCA/ICA spectral compression is reduced to ICA-based spectral compression. Since various combinations of m and n have different effects on the performance of mixed PCA/ICA spectral compression in different applications, experiments conducted for subpixel detection and mixed pixel classification and quantification are used to evaluate performance.

It is worth noting that the main theme of this paper is a transform that performs spectral compression, not just spatial compression. The development of new techniques for

spatial compression is not our major interest, since there are already many well-known spatial compression techniques such as SPIHT, SPECK, and JPEG 2000 available in open public domain. In view of that, discussions on spatial compression, which can be found in many references in the literature, are not included in this paper to avoid blurring our main focus. Nevertheless, it should be noted that any spatial compression technique can be used to be implemented in conjunction with our proposed mixed PCA/ICA transform to perform both spectral and spatial compression.

This paper is organized as follows. Section 2 develops the new mixed PCA/ICA approach to spectral-spatial compression for hyperspectral imagery. Section 3 presents experiments for performance evaluation. Section 4 concludes with some remarks.

2 Mixed PCA/ICA

PCA⁷ is a versatile, widely used transform in applications ranging from sample spatial or spectral decorrelation to data compression to dimensionality reduction. Since the sample covariance matrix used by the PCA consists of second-order statistics, the PCA is considered as a second-order-statistics-based transform, which can only preserve information characterized by second-order statistics throughout the transformation. In many applications preserving information of second-order statistics is generally not sufficient for substance characterization in small objects, rare targets, etc., which generally requires statistics of orders higher than 2. Under such a circumstance, the PCA transform may not be effective. ICA⁹ has been widely used to cope with this problem. For ICA to be effective, two assumptions must be satisfied. One crucial assumption is that all the signal sources must be random sources. Since a linear sum of a finite number of Gaussian signal sources is still Gaussian, a second crucial assumption is that at most one signal source can be Gaussian. Because of this particular assumption, ICA is able to capture information that is characterized by non-Gaussianity (i.e., super-Gaussianity or sub-Gaussianity) whose statistics goes beyond the second order. Therefore, a logical and natural approach to preserving statistics of second and higher order is to combine the PCA and the ICA into one transform so as to retain the strengths of both.

However, developing such a combination seems more easily said than done. This is because four key issues need to be addressed before mixing the PCA and ICA. One is how many components required for a mixed PCA/ICA transform to retain, i.e., how many principal components (m) and how many independent components (n) the result being called an (m, n) -PCA/ICA transform. This same issue is also encountered in both the PCA and ICA transforms. However, unlike the PCA, which ranks PCs according to eigenvalues in decreasing order, ICA does not prioritize the ICs it generates. So, a second issue is which n ICs should be selected for the (m, n) -PCA/ICA transform. Selecting appropriate ICs is crucial. A third issue is how to combine the two different sets of projection vectors, PCA-generated eigenvectors and ICA-generated projection vectors, since these vectors are generated by different orders of statistics

and are not necessarily the same. A fourth issue is how to decompress the mixed $p=m+n$ component images to reconstruct the original image.

The four mentioned issues can be addressed as follows:

1. The first can be addressed by the new concept of VD, recently developed in Refs. 10 and 11, which was shown to be effective for dimensionality reduction.^{8,12} We can use the VD-estimated value for p .
2. The second can be addressed as in Ref. 8, where three algorithms were developed to rank ICs by different criteria, as the PCA does for its PCs with variance used as a criterion. Of particular interest the use of an unsupervised algorithm, called the automatic target generation process (ATGP),^{10,15} to produce an appropriate set of initial projection vectors for the ICA so that the generated ICs can be ranked in the same order as the initial projection vectors generated by the ATGP. An ATGP-based algorithm has been shown to be promising in Ref. 8 and is used in our proposed (m, n) -PCA/ICA transform.
3. In order to address the third issue one first determines the number m of PCs resulting from the PCA to select. Let $\{\mathbf{v}_{ij}\}_{j=1}^m$ be the eigenvectors that generate the first m PCs. Then all data samples are projected to a space orthogonal to the space spanned by the m eigenvectors, denoted by $\langle \{\mathbf{v}_{ij}\}_{j=1}^m \rangle^\perp$. Then the ATGP-based ICA is applied to the space $\langle \{\mathbf{v}_{ij}\}_{j=1}^m \rangle^\perp$ to find the first n ICs with their corresponding projection vectors, denoted by $\{\mathbf{z}_{i1}\}_{i=1}^n$. Combining the m eigenvectors $\{\mathbf{v}_{ij}\}_{j=1}^m$ with the n projection vectors $\{\mathbf{z}_{i1}\}_{i=1}^n$ yields a new set of basis vectors $\{\mathbf{w}_{ij}\}_{i=1}^p$ that can be used for our desired (m, n) -PCA/ICA transform, where $\mathbf{w}_i = \mathbf{v}_i$ for $1 \leq i \leq m$, $\mathbf{w}_{i+m} = \mathbf{z}_i$ for $1 < i < n$, and $p = m + n$.
4. Finally, the fourth issue can be addressed by using $\{\mathbf{w}_{ij}\}_{i=1}^p$ just obtained to decompress the compressed image and thus reconstruct the original image.

Once all the four issues are solved, a mixed (m, n) -PCA/ICA transform can be developed for spectral-spatial compression as follows.

Mixed (m, n) -PCA/ICA spectral compression-decompression algorithm.

1. Use the VD to estimate the number of components needed to be retained for spectral compression, denoted by p .
2. Perform the PCA to find eigenvalues $\{\lambda_{ij}\}_{i=1}^L$ and their corresponding eigenvectors $\{\mathbf{v}_{ij}\}_{i=1}^L$, retain m PCs with the m largest eigenvalues, and set $\mathbf{V} = \{\mathbf{v}_{ij}\}_{i=1}^m$.
3. Define an $(L-m) \times (L-m)$ eigenvalue diagonal matrix by

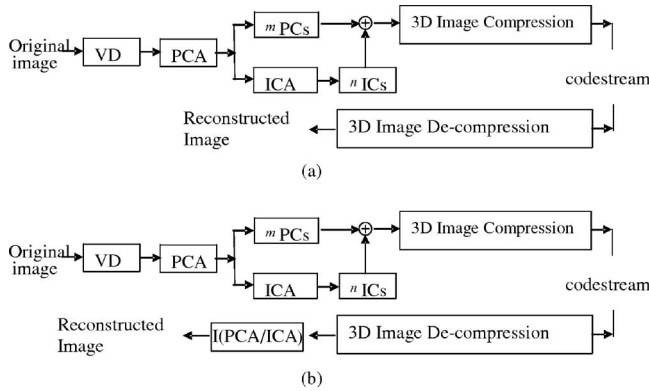


Fig. 1 Structure of mixed (m,n) -PCA/ICA transform: (a) compression, (b) decompression.

$$\mathbf{D} = \begin{bmatrix} \lambda_{m+1} & 0 & 0 \\ 0 & \ddots & 0 \\ \mathbf{0} & 0 & \lambda_L \end{bmatrix},$$

and an $L \times (L-m)$ eigenvector matrix by $\mathbf{E} = [\mathbf{v}_{m+1} \ \mathbf{v}_{m+2} \ \cdots \ \mathbf{v}_L]$. A whitening matrix $\mathbf{D}^{-1/2} \mathbf{E}^T$ is then used to sphere the mean-removed data matrix \mathbf{X} . Let the resulting matrix $\hat{\mathbf{X}} = \mathbf{D}^{-1/2} \mathbf{E}^T \mathbf{X}$ be denoted by $\hat{\mathbf{X}}$.

4. Apply FastICA,⁹ using the $n=p-m$ ATGP-generated pixel vectors as initial projection vectors, to the sphered data $\hat{\mathbf{X}}$ to generate n projection vectors, denoted by $\{\mathbf{z}_j\}_{j=1}^n$, as well as n ICs. Let \mathbf{Z} denote the projection matrix formed by $\mathbf{Z} = [\mathbf{z}_1 \ \mathbf{z}_2 \ \cdots \ \mathbf{z}_n]$ with dimensionality $(L-m) \times n$, and define $\hat{\mathbf{Z}} = \mathbf{Z}^T \mathbf{D}^{1/2} \mathbf{E}^T$.
5. Form a new image cube \mathbf{Y} by the m PCs and the n ICs, and let $\mathbf{W} = [\mathbf{V} \ \hat{\mathbf{Z}}]$.
6. Apply the inverse PCA, $\mathbf{X} = \mathbf{W}^{-1} \mathbf{Y}$, and add the mean back to reconstruct \mathbf{X} . Since p is generally (much) smaller than L , the inverse of \mathbf{W} is always taken as its pseudoinverse.

Figure 1 depicts a block diagram of a mixed (m,n) -PCA/ICA transform for data compression, where $\mathbf{I}(\text{PCA-ICA})$ in Fig. 1(b) denotes the inverse of the mixed (m,n) -PCA/ICA transform via the projection vectors $\{\mathbf{w}_{il}\}_{l=1}^p$.

3 Experiments

In this section, we report on the use of two sets of image data for experiments to evaluate the performance of a mixed (m,n) -PCA/ICA transform for data compression with various combination (m,n) .

3.1 HYDICE Image Experiments

The first image to be studied is the Hyperspectral Digital Imagery Collection Experiment (HYDICE) image scene shown in Fig. 2(a), which has a size of 64×64 pixel vectors with 15 panels in the scene, and the ground truth map in Fig. 2(b). It was acquired in 210 spectral bands with a spectral coverage from 0.4 to 2.5 μm . Low-signal, high-

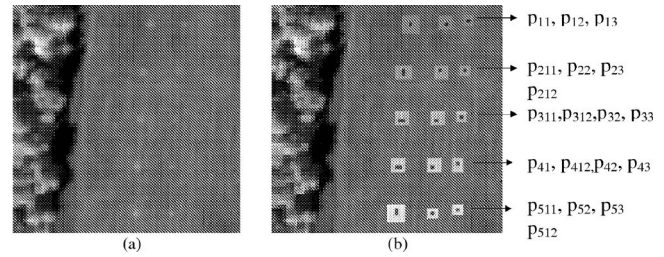


Fig. 2 (a) A HYDICE panel scene that contains 15 panels; (b) ground truth map of spatial locations of the 15 panels.

noise bands (bands 1 to 3 and 202 to 210) and water vapor absorption bands (bands 101 to 112 and 137 to 153) were removed. So a total of 169 bands were used in the experiments. The spatial resolution is 1.56 m, and spectral resolution is 10 nm. The spatial resolution of the image scene suggests that the panels in the second and third columns, denoted by $p_{12}, p_{13}, p_{22}, p_{23}, p_{32}, p_{33}, p_{42}, p_{43}, p_{52}, p_{53}$ in Fig. 2(b), are one pixel in size. Additionally, except for the panel in the first row and first column (denoted by p_{11}), which also has a size of one pixel, all other panels located in the first column are two-pixel panels: the panel in the second row, with two pixels lined up vertically, denoted by p_{211} and p_{212} ; the panel in the third row, with two pixels lined up horizontally, denoted by p_{311} and p_{312} ; the panel in the fourth row, with two pixels also lined up horizontally, denoted by p_{411} and p_{412} ; and the panel in the fifth row, with two pixels lined up vertically, denoted by p_{511} and p_{512} . Since the size of the panels in the third column is 1×1 m, they cannot be seen in Fig. 2(a), because that size is less than the 1.56-m pixel resolution.

First of all, we need to determine the number of components, denoted by p , required for the mixed PCA/ICA transform to retain the image scene in Fig. 2(a). It has been shown that $\text{VD} = 9$ with the false-alarm probability fixed at $P_F = 10^{-3}$ or 10^{-4} was appropriate for dimensionality reduction.⁸ Therefore, $\text{VD} = 9$ was also used for our experiments.

In what follows, five scenarios of mixed PCA/ICA transforms, with $(m=9, n=0)$ (i.e., PCA), $(m=0, n=9)$ (i.e., ICA), $(m=1, n=8)$, and $(m=2, n=7)$, were investigated for applications in mixed pixel classification and quantification, where unsupervised fully constrained least squares (UFCLS)^{10,16} was used to evaluate their performance on compressed and decompressed domains, and where the number of classes to be classified was set to $p=9$. The reasons for using UFCLS are two. One is that linear spectral mixture analysis (LSMA) is a widely used image analysis technique. The other is that data compression is generally carried out without prior knowledge. When the UFCLS was implemented, the target knowledge was assumed to be unknown, and all necessary target information was generated by the UFCLS. According to Refs. 10 and 16, 34 target pixels were enough to provide such knowledge, and so 34 were used for mixed pixel classification and quantification for the HYDICE image in Fig. 2, which was the original hyperspectral image cube. Therefore, the UFCLS was first applied to the original HYDICE image with p set to 34 for benchmark comparison, and Fig. 3 shows the mixed pixel

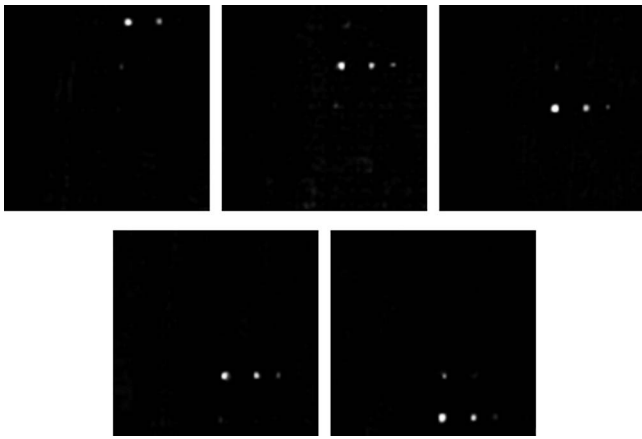


Fig. 3 Fifteen-panel classification by the UFCLS on the original image cube.

classification results; only five of the images that classified the 15 panels are shown. It should be noted that since the panels in rows 2 and 3 were made of the same material with different paints, the detection of panels in row 2 might imply the detection of panels in row 3, and vice versa. The same is true for detection of the panels in rows 4 and 5.

Experiment 1 [scenario 1: PCA ($m=9, n=0$)]

In this experiment, the mixed PCA/ICA transform is reduced to the standard PCA transform. Figure 4 shows the nine PCA-generated PCs. Figures 5 and 6 show the results produced by the UFCLS in the 15-panel classification using nine PC-compressed and -decompressed image cubes, respectively.

As demonstrated in Figs. 5 and 6, the UFCLS performed very poorly in classification of the 15 panels in the scene.

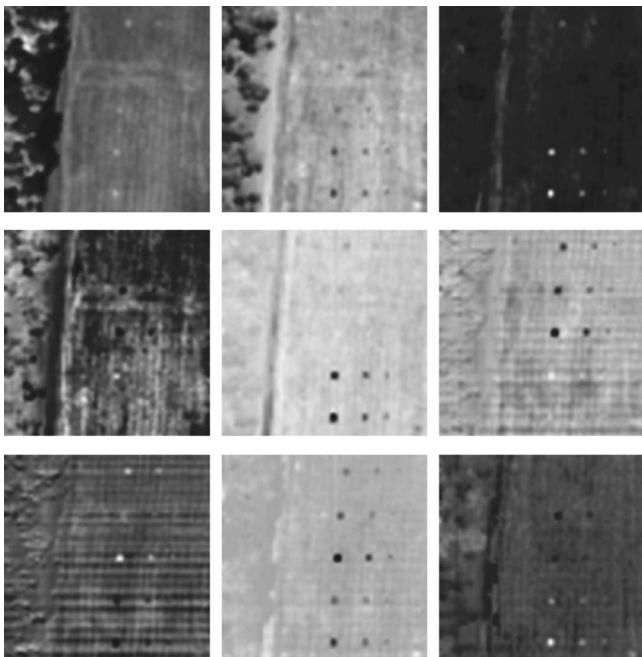


Fig. 4 The nine principal components.

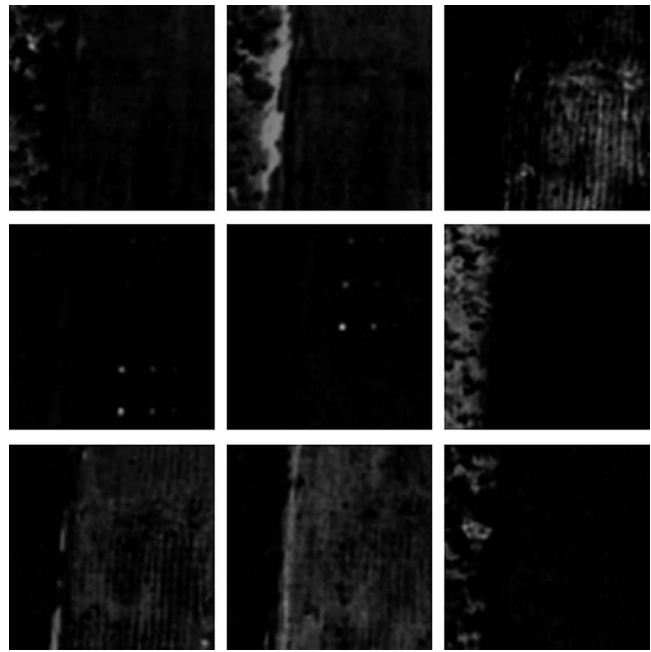


Fig. 5 Classification by the UFCLS using the nine PCs in Fig. 4.

Comparing the results in Figs. 5 and 6, against that in Fig. 3, we see that the PCA-based spectral-spatial compression failed to capture subtle details of the 15 panels. This is primarily due to the fact that the PCA-based spectral compression is a second-order-statistics-based transform, which largely characterizes background information in Figs. 5 and 6, but not panel information, which is generally preserved by high-order statistics, as demonstrated in the following example. As also demonstrated in Figs. 5 and 6, the results

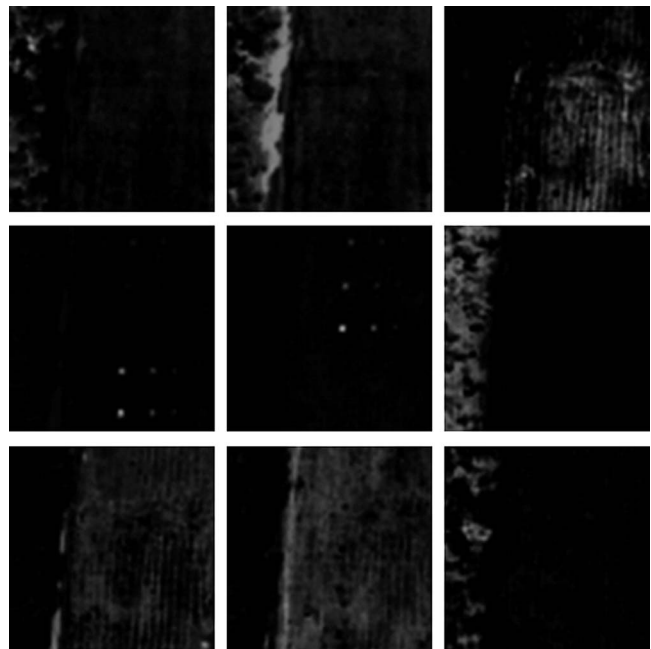


Fig. 6 Fifteen-panel classification by the UFCLS on the PCA-decompressed image cube obtained by using the nine PCs in Fig. 4.

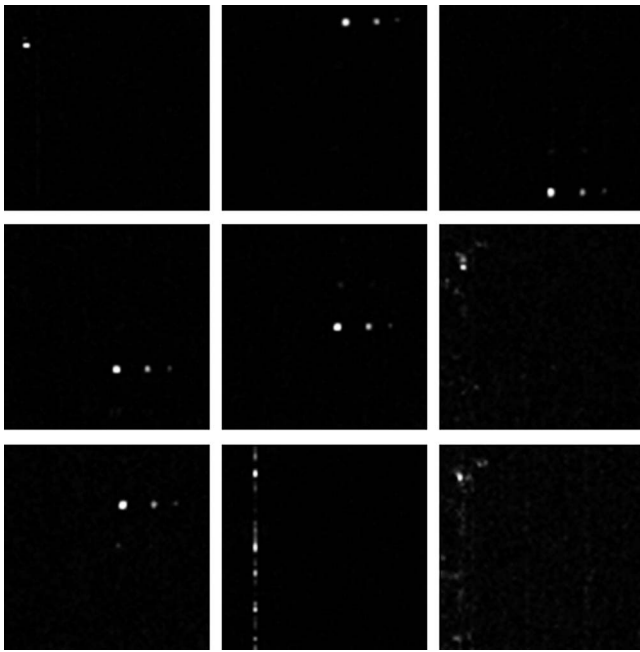


Fig. 7 The nine independent components.

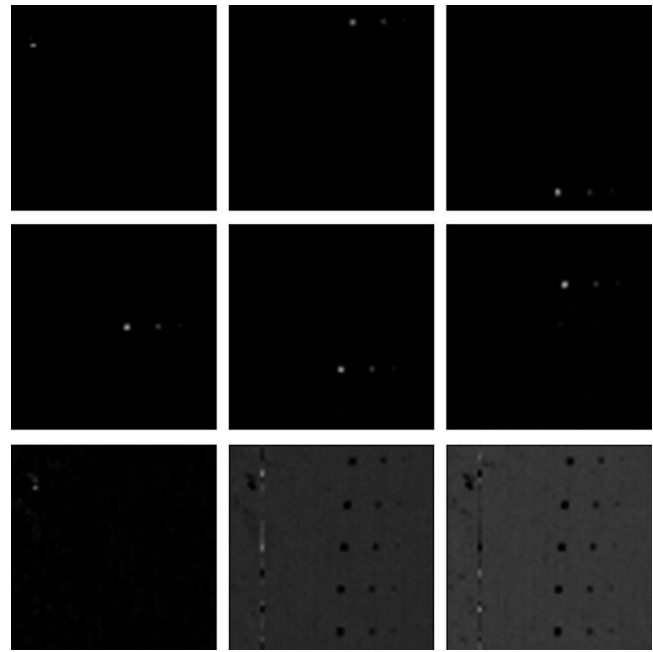


Fig. 8 Classification by the UFCLS using the nine ICs in Fig. 7.

produced by using the nine PC-decompressed image cubes showed little improvement in panel detection and classification. This implies that the decompressed image cube reconstructed by the nine PCs seemed to provide no significant advantage in target detection and mixed pixel classification.

Experiment 2 [scenario 2: ICA ($m=0, n=9$)]

As a complete opposite of scenario 1 in Experiment 1, this experiment considers another scenario, called scenario 2, where the nine components used for mixed pixel classification were the ICs shown in Fig. 7, obtained from FastICA using the ATGP-generated initial projection vector.¹⁵ Evidently, the nine ICs in Fig. 7 have already extracted all the 15 panels, while the background information preserved in Fig. 4 seems not to appear in these nine ICs. Figures 8 and 9 show the results produced by the UFCLS in the 15-panel classification using the nine IC-compressed and -decompressed image cubes, respectively; we see that the UFCLS performed better using ICA than using PCA (Figs. 5 and 6) in terms of panel target detection.

Experiment 3 [scenario 3: ($m=1, n=8$)-PCA/ICA transform]

Experiment 1 and 2 demonstrated advantages and disadvantages of the PCA and of the ICA transform used for compression. This experiment investigates a scenario, called scenario 3, to see how much gain can be obtained by the proposed mixed (m, n)-PCA/ICA transform.

In order to see the performance of the mixed (1,8)-PCA/ICA transform in mixed pixel classification, Figs. 10 and 11 show the 15-panel classification results by the UFCLS using image cubes compressed and decompressed, respectively, by the (1,8) mixed-component transform. The results in Fig. 10, obtained by using the compressed image cube,

seem slightly better than those in Fig. 11, obtained by using the decompressed image cube, in classification of the 15 panels, particularly the panels in rows 2 and 3. But the results shown in Fig. 11 are closer to the UFCLS result obtained from the original image cube shown in Fig. 3 and also included more extracted background classes than that in Fig. 10.

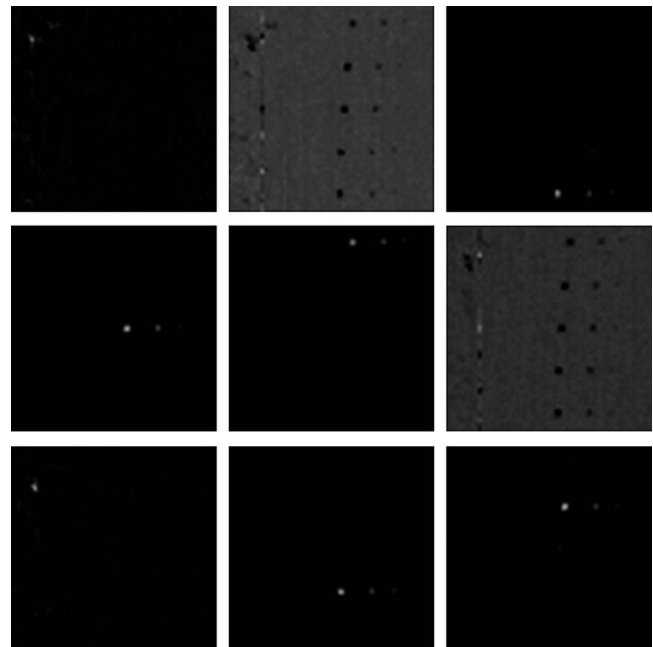


Fig. 9 Classification by the UFCLS using the ICA-decompressed image cube obtained by using the nine ICs in Fig. 7.

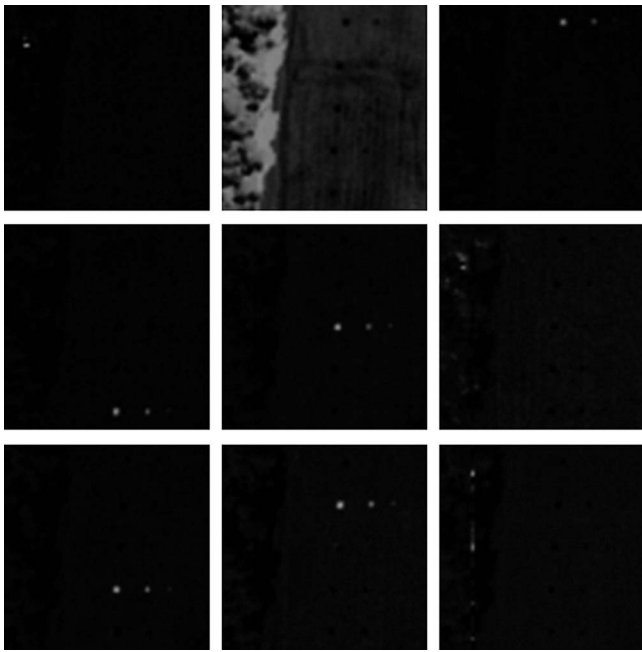


Fig. 10 Classification by the UFCLS using nine mixed components.

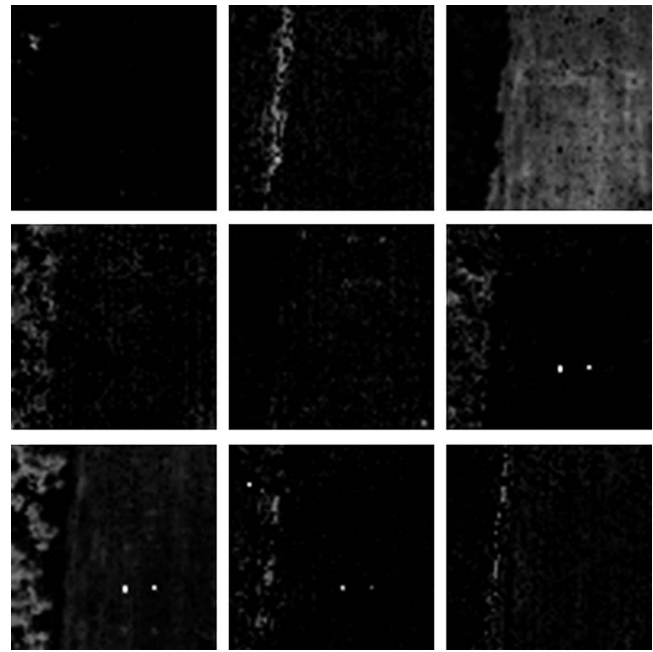


Fig. 12 Classification by the UFCLS using nine mixed components.

Experiment 4 [scenario 4: ($m=2, n=7$)-PCA/ICA transform]

This experiment further investigates another scenario, called scenario 4, to see if a further improvement can be gained by increasing the one PC to two PCs while reducing the eight ICs to seven ICs, resulting in a mixed (2,7)-PCA/ICA transform. Figures 12 and 13 show the 15-panel classification results by the UFCLS using the compressed and

decompressed image cubes, respectively; the UFCLS performed poorly in 15-panel classification in both cases.

This experiment demonstrated that adding one more PC could do more harm than good for UFCLS mixed pixel classification. This was because the first PC was sufficient to capture second-order statistics, and adding a second PC did not provide useful information for panel detection and classification, but rather obscured the panel information.

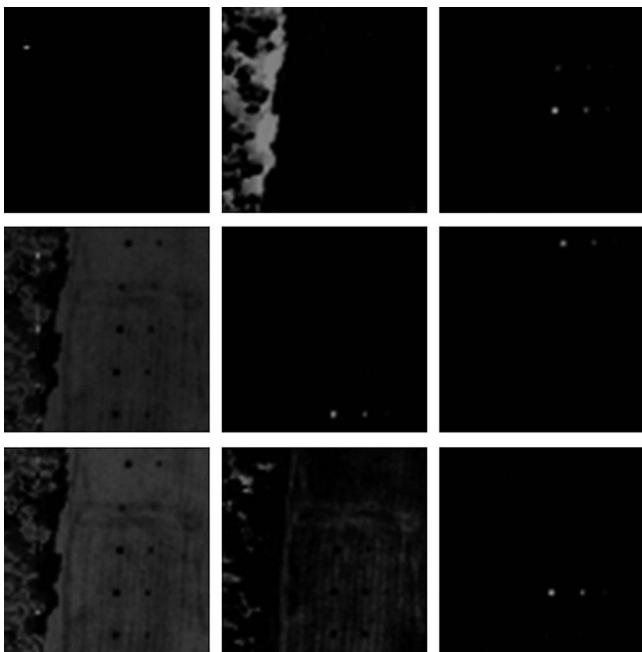


Fig. 11 Classification by the UFCLS on the (1,8)-PCA/ICA-decompressed image cube obtained by using nine mixed components.

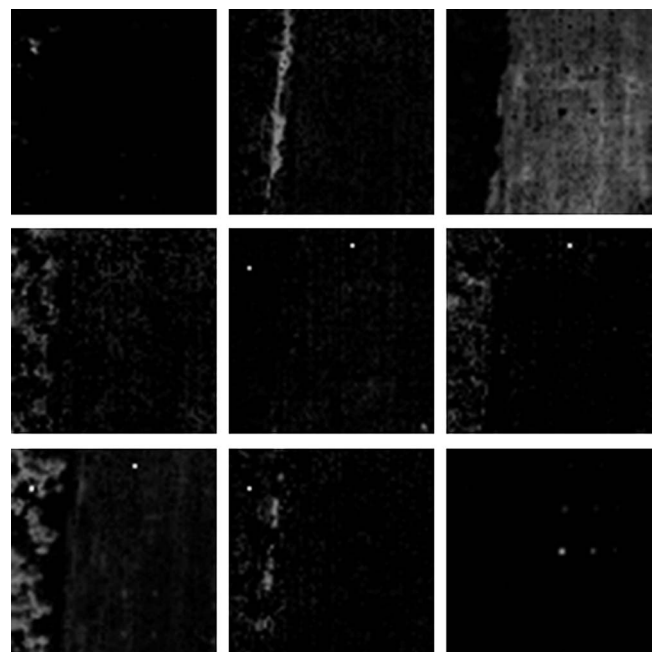


Fig. 13 Classification by the UFCLS on the PCA/ICA-decompressed image cube obtained by using nine mixed components.

Table 1 LSEs calculated for Experiments 1 to 4.

(m, n)	LSE
(9, 0)	3.25×10^4
(0, 9)	4.24×10^7
(1, 8)	8.07×10^6
(2, 7)	3.83×10^5

Finally, the least-squares errors (LSEs) were calculated for the four scenarios that were conducted in the preceding four experiments using mixed (m, n) -PCA/ICA transforms with $(m, n) = (9, 0)$, $(0, 9)$, $(1, 8)$, and $(2, 7)$. The results are tabulated in Table 1. As clearly shown there, the LSE is increased as more PCs were replaced by ICs; the smallest and largest LSEs were produced by $(9, 0)$ -PCA and $(0, 9)$ -ICA, respectively. However, the worst performance in mixed pixel classification came from $(9, 0)$ -PCA and $(2, 7)$ -PCA/ICA, which yielded smaller LSEs than $(0, 9)$ -ICA and $(1, 8)$ -PCA/ICA, which performed significantly better in the 15-panel classification but produced larger LSEs. This evidence demonstrates that a smaller LSE did not necessarily produce better performance in mixed pixel classification. It further suggested that the LSE might not be an appropriate measure for hyperspectral data compression.

Experiment 5 (mixed pixel quantification)

The preceding four experiments were evaluated qualitatively by visual assessment. It is very difficult to see how a mixed (m, n) -PCA/ICA transform performs quantitatively. To do so, we conducted this experiment to evaluate the performance of a mixed (m, n) -PCA/ICA transform in mixed pixel quantification for the 15 panels in Fig. 2. Among the four scenarios, only scenarios 2 and 3 successfully classified 15 panels, so only the results produced by the $(0, 9)$ -PCA/ICA transform and the $(1, 8)$ -PCA/ICA transform were used for mixed pixel quantification analysis. Table 2 tabulates their abundance quantification of the 15 panels obtained in Figs. 8 and 9 and in Figs. 10 and 11, respectively; the results for abundance quantification of the 15 panels obtained by applying the UFCLS to the original image cube in Fig. 3 are also included for benchmark comparison. As noted, the subpixel panels p_{13} , p_{23} , p_{33} , p_{43} , and p_{53} in Fig. 2(b) have a size of $(1 \times 1 \text{ m})$ smaller than the $1.56 \times 1.56\text{-m}$ spatial resolution. This indicates that the size of these five subpixel panels is approximately $1/(1.56 \text{ m})^2 = 0.41091 \text{ m}^2$, which is equivalent to saying that the abundance fractions of these three subpixels present in a single pixel were close to 0.41091. With this interpretation, Table 2 shows that both the mixed $(1, 8)$ -PCA/ICA transforms performed slightly better than the mixed $(0, 9)$ -PCA/ICA transform in the 15-panel abundance quantification where the UFCLS results obtained on the reconstruction image based on $(1, 8)$ -PCA/ICA had the closest results to the UFCLS results produced using the original image cube.

One remark is noteworthy. The $VD=9$ used in the experiments is only an estimate and not necessarily exact. According to our extensive experiments on the HYDICE panel scene in Fig. 2, for dimensionality reduction $VD=9$ is appropriate. However, since the value estimated by the VD is fixed, the $VD=9$ used for dimensionality reduction may not be appropriate for other applications such as band selection.^{13,17} This is because different applications require different false-alarm probabilities. So we can always vary the estimate of the VD by varying the false-alarm probability at different thresholding levels. We can thus make the VD adaptable to various applications.¹⁸ Keeping this in mind, $VD = 9$ may be effective for dimensionality reduction, but it may not be appropriate for data compression, because using ICA alone may not preserve background information and using PCA alone may miss information of small objects. Of course, if p is sufficiently large, PCA and ICA can perform well. However, for a smaller p , neither may work well, as demonstrated by our experiments. In this case, our proposed mixed PCA/ICA transform may still work well for the same p . This provides evidence that the mixed PCA/ICA transform has advantages over the PCA and ICA in combining their strengths.

3.2 AVIRIS Image Experiments

The second image to be studied is an Airborne Visible Infrared Imaging Spectrometer (AVIRIS) image scene, which was collected from the Cuprite mining site, Nevada, in 1997 and is shown in Fig. 14. It is a 224-band AVIRIS image scene with size 350×350 pixels and well understood mineralogically, and has reliable ground truth in the form of a library of mineral spectra, collected at the site by USGS and available on its Web site.¹⁹ The five minerals, alunite (A), buddingtonite (B), calcite (C), kaolinite (K), and muscovite (M), are specified by pixels white-circled and labeled by A, B, C, K, and M in Fig. 14(b) according to the ground truth provided by the USGS. The spectrum profiles for these five signatures are plotted in Fig. 14(c) and labeled likewise. It should be noted that bands 1 to 3, 105 to 115, and 150 to 170 had been removed prior to the analysis due to water absorption and low SNR in those bands. As a result, a total of 189 bands were used for experiments. Since all similar experiments conducted for HYDICE data can be also applied to these AVIRIS data, only mixed pixel quantification was studied for quantitative analysis, for illustration, to demonstrate that the proposed mixed PCA/ICA is a general approach and also works for any hyperspectral data.

In order to simplify our experiment, only one quarter of the image, at the bottom right corner in Fig. 14(a), was selected for study, and it is shown in Fig. 15(b) with four 3×3 simulated panels implanted at the bottom left corner in such a way that the implanted panel pixels replaced their corresponding real image pixels. In other words, the image scenes in Figs. 14(b) and 15(b) are identical except that there are 36 simulated pixels (9 pixels for each panel) implanted in Fig. 15(b) to replace the original 36 real-image pixels in Fig. 14(b). These four panels, denoted by p_{ij} for $i=1, 2$ and $j=1, 2$, were simulated in accordance with the compositions of signatures specified in Table 3, where row and column indices are indicated by i and j , and the background (BKG) is specified by the signatures of the real-

Table 2 Abundance quantification by UFCLS using mixed (m,n) -PCA/ICA spectral spatial compression.

Panel	$(m=1, n=8)$ -PCA/ICA		$(m=0, n=9)$ -PCA/ICA		UFCLS ($p=34$)
	Compressed	Decompressed	Compressed	Decompressed	
p_{11}	1	1	1	1	1
p_{12}	0.4748	0.4419	0.4708	0.4283	0.4098
p_{13}	0.2175	0.1542	0.2166	0.1721	0.0499
p_{211}	0.9748	0.3438	1	1	0.5255
p_{221}	1	0.3424	0.9853	0.9191	0.3141
p_{22}	0.9031	0.2890	0.9181	0.9051	0.6917
p_{23}	0.3652	0.1112	0.3751	0.248	0.4221
p_{311}	0.8372	0.9326	0.844	0.7569	0.8647
p_{312}	1	1	1	1	1
p_{32}	0.5615	0.5439	0.5647	0.4946	0.5343
p_{33}	0.3859	0.3406	0.3929	0.3122	0.3285
p_{41}	1	1	1	0.466	1
p_{412}	0.8928	0.9019	0.8991	0.5501	0.3821
p_{42}	0.8052	0.7936	0.7974	0.8361	0.7034
p_{43}	0.2622	0.1986	0.2489	0.2596	0.2242
p_{511}	0.7265	0.6956	0.7252	0.5846	0.7203
p_{521}	1	1	1	1	1
p_{52}	0.7386	0.7294	0.7349	0.724	0.7789
p_{53}	0.1982	0.1368	0.1812	0.1213	0.1466

image pixels in the scene that were replaced by their corresponding implanted pixels. For example, all nine pixels in panel p_{12} were simulated by the 50% calcite and 50% BKG signature specified by their replaced real image pixels. So, all of these nine simulated panel pixels contained 50% calcite, but different BKG signatures. Two benefits can be gained from our designed experiments. One is that the data are available on a Web site, so that whoever is interested in our proposed method can repeat what we did in the experiments for comparison with new algorithms. The other benefit is that all parameters used to simulate the panels are

Table 3 Compositions of four simulated panels.

Pixels	Signatures	Composition
9 in p_{11}	Calcite	100% calcite+0% BKG
9 in p_{12}	Calcite, BKG	50% calcite+50% BKG
9 in p_{21}	Kaolinite	100% kaolinite+0% BKG
9 in p_{22}	Kaolinite, BKG	50% kaolinite+50% BKG

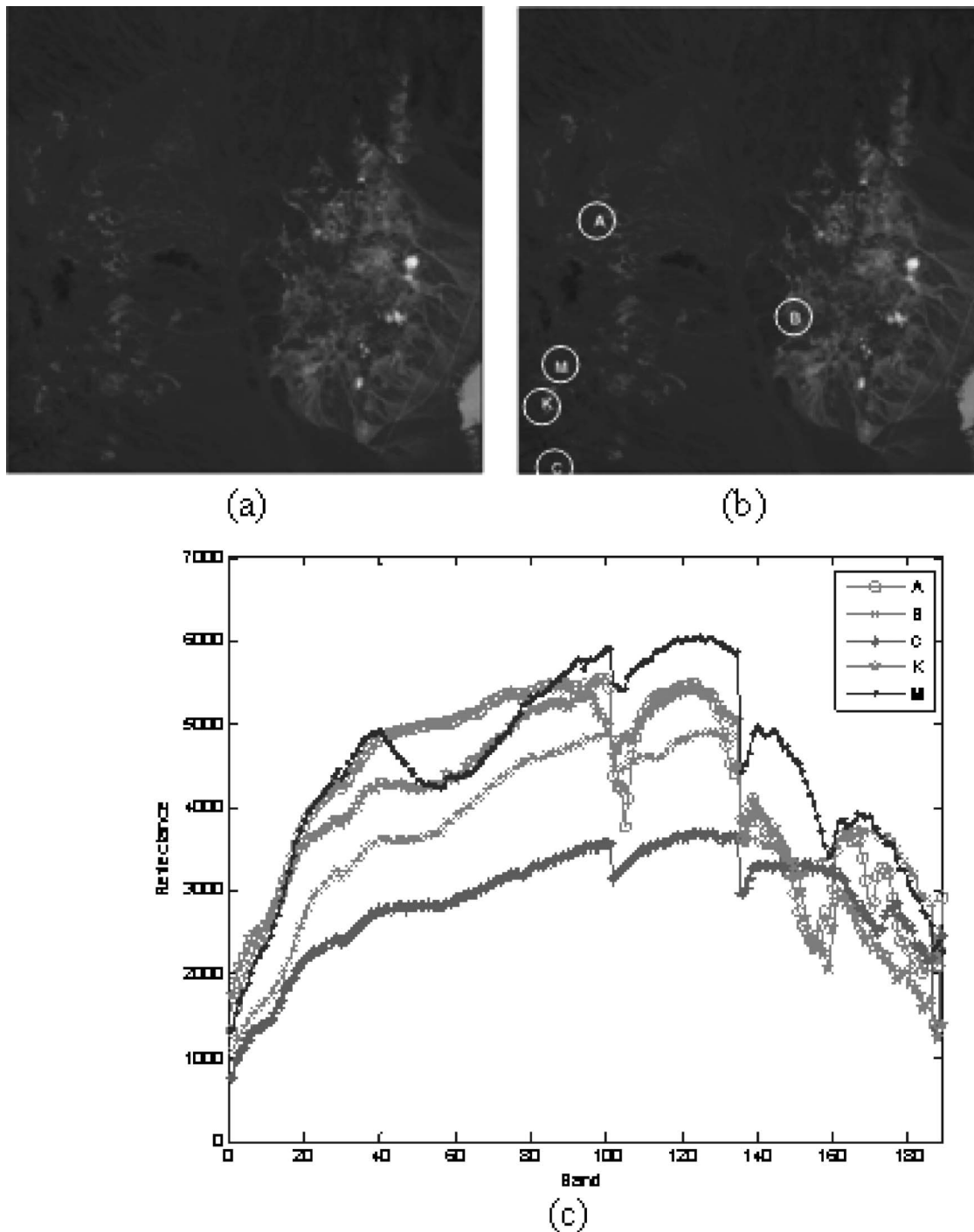


Fig. 14 (a) Spectral band 50 (827 nm) of the Cuprite AVIRIS image scene. (b) Spatial positions of five pure pixels corresponding to minerals: alunite (A), buddingtonite (B), calcite (C), kaolinite (K), and muscovite (M). (c) Spectra of five pure pixels corresponding to the five minerals.

fully controlled, so that performance analysis is conducted impartially and objectively. The VD estimated for the image scene in Fig. 15(b) was 10, with the false-alarm probability set at $P_F=10^{-3}$. By virtue of $VD=10$ and the 36 panel pixels simulated in Table 3, a detailed analysis for their quantification can be conducted by the UFCLS using PCA only, ICA only, and mixed PCA/ICA transforms.

Interestingly, the quantitative results obtained by the UFCLS for panels in row 1 and row 2 were quite different and are analyzed as follows:

1. For panel pixels in the first panel p_{11} in row 1, simulated by the 100% mineral signature calcite, the UFCLS only using PCA [i.e., (10,0)-PCA/ICA] could

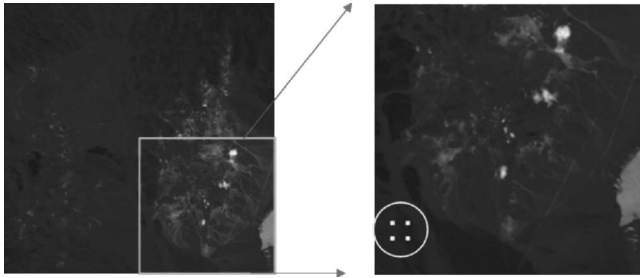


Fig. 15 Spatial locations of four implanted panels.

not detect any of the nine pure panel pixels in p_{11} , while the UFCLS was able to detect and quantify all nine panel pixels with correct 100% abundance of calcite if the ICA-only [i.e., (0,10)-PCA/ICA] and the mixed (1,9)-PCA/ICA transform were used.

2. For the panel pixels in the second panel p_{12} in row 1, Table 4 tabulates UFCLS-estimated abundance fractions of the calcite contained in the nine panel pixels in the second panel p_{12} in row 1. There were no results for the PCA, since it missed all nine panel pixels. Figure 16 shows graphical representations of the abundances in Table 4 for visual assessment. It clearly shows that the (1,9)-PCA/ICA transform performed significantly better than the (0,10)-PCA/ICA.
3. For panel pixels in the first panel p_{21} in row 2 simulated by the 100% mineral signature kaolinite, the UFCLS using all the three different transforms successfully detected and quantified all nine panel pixels with correct 100% abundance of kaolinite. According to the ground truth provided by the USGS, the major background for this scene is made up of a mixture of alunite and kaolinite. As a result, PCA was able to pull out some information on kaolinite from the panel

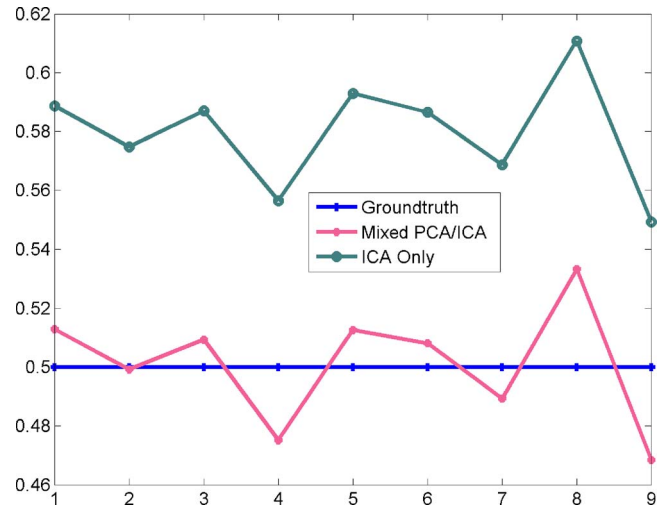


Fig. 16 Graphical representation of Table 4 for visual assessment.

p_{21} . This was different from the results obtained from the panel p_{11} , where all nine pixels were made up by 100% calcite, which was not part of the image background. In this case, the calcite could not be extracted by the second-order-statistics transforms; it could be only extracted by the high-order-statistics-based transforms.

4. For the nine panel pixels in the second panel p_{22} in row 2, Table 5 tabulates UFCLS-estimated abundance fractions of kaolinite. Figure 17 shows graphical representations of the abundances in Table 5 for visual assessment. According to Fig. 17, the mixed PCA/ICA (1,9) transform was best among all the three transforms, the (0,10)-PCA/ICA transform was next, and the (10,0)-PCA/ICA transform was the worst.

Table 4 UFCLS-estimated abundance fractions of calcite contained in nine panel pixels in p_{12} in row 1.

50% calcite in pixel	Abundance (%)		
	PCA only ($m=10, n=0$)	ICA only ($m=0, n=10$)	Mixed PCA/ICA ($m=1, n=9$)
1	—	58.87	51.29
2	—	57.48	49.92
3	—	58.70	50.94
4	—	55.65	47.52
5	—	59.30	51.26
6	—	58.65	50.81
7	—	56.87	48.93
8	—	61.08	53.34
9	—	54.93	46.85

Table 5 UFCLS-estimated abundance fractions of kaolinite contained in nine panel pixels in p_{22} in row 2.

50% kaolinite in pixel	Abundance (%)		
	PCA only ($m=10, n=0$)	ICA only ($m=0, n=10$)	Mixed PCA/ICA ($m=1, n=9$)
1	53.94	52.54	50.29
2	50.79	53.57	51.11
3	55.75	50.89	48.61
4	51.80	51.50	49.00
5	54.00	52.81	50.55
6	52.06	51.18	48.98
7	52.04	52.02	49.92
8	52.86	53.53	50.96
9	51.56	51.55	49.38

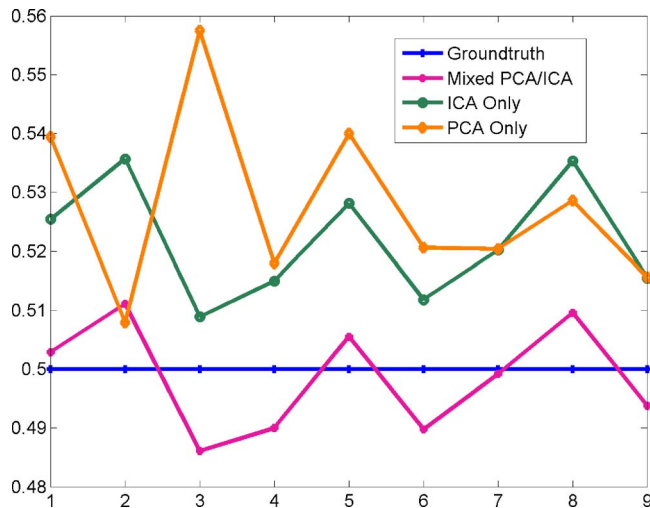


Fig. 17 Graphical representation of Table 5 for visual assessment.

Other experiments similar to those conducted for the HYDICE data in Sec. 3.1 were also performed for the AVIRIS data to see if there were differences in performance using two different data sets. The conclusions were similar. Due to limited space, those results are not included in this paper to avoid duplication.

4 Conclusions

This paper presents a mixed (m,n) -PCA/ICA transform, which can be considered as a generalization of the PCA and ICA. It adjusts the two parameters m and n by retaining the first m PCs produced by the PCA to capture different levels of information on second-order statistics, and n ICs generated by the ICA to preserve different degrees of information on statistical independence. Furthermore, a recently developed concept, VD, is also introduced into the proposed mixed (m,n) -PCA/ICA transform to estimate the total number of components, p , used in the transform, with $p=m+n$. Experimental results demonstrate that the mixed (m,n) -PCA/ICA transform performs better than the PCA and ICA alone in subpixel detection and in mixed pixel classification and quantification, provided that the parameters m and n are selected appropriately.

References

1. D. S. Taubman and M. W. Marcellin, *JPEG2000: Image Compression Fundamentals, Standard and Practice*, Kluwer, Boston (2002).
2. ISO, *Information Technology—JPEG 2000 Image Coding System—Part 1: Core Coding System*, ISO, Geneva (2002).
3. ISO, *Information Technology—JPEG 2000 Image Coding System—Part 2: Extensions; Final Committee Draft*, ISO, Geneva (2000).
4. B.-J. Kim, Z. Xiong, and W. A. Pearlman, "Low bit-rate scalable video coding with 3-D set partitioning in hierarchical trees (3-D SPIHT)," *IEEE Trans. Circuits Syst. Video Technol.* **10**(8), 1374–1387 (2000).
5. A. Said and W. A. Pearlman, "A new, fast, and efficient image codec based on set partitioning in hierarchical trees," *IEEE Trans. Circuits Syst. Video Technol.* **6**(3), 243–250 (1996).
6. B. Ramakrishna, A. Plaza, C.-I. Chang, H. Ren, Q. Du, and C.-C. Chang, "Spectral/spatial hyperspectral image compression," in *Hyperspectral Data Compression*, G. Motta and J. Storer, Eds., Springer-Verlag (2005).
7. J. Richards and X. Jia, *Remote Sensing Digital Image Analysis*, 3rd ed., Springer-Verlag (1999).
8. J. Wang and C.-I. Chang, "Independent component analysis-based di-

mensionality reduction with applications in hyperspectral image analysis," *IEEE Trans. Geosci. Remote Sens.* **44**(6), 1586–1600 (2006).

9. A. Hyvarinen, J. Karhunen, and E. Oja, *Independent Component Analysis*, John Wiley & Sons (2001).
10. C.-I. Chang, *Hyperspectral Imaging: Techniques for Spectral Detection and Classification*, Kluwer Academic/Plenum Publishers (2003).
11. C.-I. Chang and Q. Du, "Estimation of number of spectrally distinct signal sources in hyperspectral imagery," *IEEE Trans. Geosci. Remote Sens.* **42**(3), 608–619 (2004).
12. J. Wang and C.-I. Chang, "Applications of independent component analysis in endmember extraction and abundance quantification for hyperspectral imagery," *IEEE Trans. Geosci. Remote Sens.* **44**(9), 2601–2616 (2006).
13. C.-I. Chang, "Utility of virtual dimensionality in hyperspectral signal/image processing," Chap. 1 in *Recent Advances in Hyperspectral Signal and Image Processing*, C.-I. Chang, Ed., Research Signpost, Trivandrum, Kerala, India (2006).
14. C.-I. Chang, "Exploration of virtual dimensionality in hyperspectral image analysis," in *Algorithms and Technologies for Multispectral, Hyperspectral, and Ultraspectral Imagery XII, SPIE Defense and Security Symp.*, Proc. SPIE (2006).
15. H. Ren and C.-I. Chang, "Automatic spectral target recognition in hyperspectral imagery," *IEEE Trans. Aerosp. Electron. Syst.* **39**(4), 1232–1249 (2003).
16. D. Heinz and C.-I. Chang, "Fully constrained least squares linear mixture analysis for material quantification in hyperspectral imagery," *IEEE Trans. Geosci. Remote Sens.* **39**(3), 529–545 (2001).
17. C.-I. Chang and S. Wang, "Constrained band selection for hyperspectral imagery," *IEEE Trans. Geosci. Remote Sens.* **44**(6), 1575–1585 (2006).
18. W. Liu, C.-C. Wu, and C.-I. Chang, "An orthogonal subspace projection-based estimation of virtual dimensionality for hyperspectral data exploitation," in *Algorithms and Technologies for Multispectral, Hyperspectral, and Ultraspectral Imagery XIII, SPIE Defense and Security Symp.*, Proc. SPIE (2007).
19. <http://speclab.cr.usgs.gov/cuprite.html>.



Jyh-Wen Chai received his MD degree and PhD degree in biomedical engineering from National Yang-Ming Medical School, Taipei, Taiwan, in 1984 and 2002. Currently he is an attending staff member in the Department of Radiology, Veterans General Hospital, Taichung, Taiwan.



Jing Wang received the BS degree in electrical engineering and MS degree in computer engineering from the Beijing University of Post and Telecommunications in 1998 and 2001. She also received the MS and PhD degrees in electrical engineering from the University of Maryland, Baltimore County, Baltimore (UMBC), in 2005 and 2006, respectively, and is currently with Xerox in New York. Her research interests include signal and image processing, pattern recognition, and data compression.



Chein-I Chang received his BS degree from Soochow University, Taipei, Taiwan, MS degree from the Institute of Mathematics at National Tsing Hua University, Hsinchu, Taiwan, and M.A. degree from the State University of New York at Stony Brook, all in mathematics. He also received his MS and MSEE degrees from the University of Illinois at Urbana-Champaign, and his PhD degree in electrical engineering from the University of Maryland, College Park. Dr. Chang has been with the University of Maryland, Baltimore County (UMBC) since 1987 and is currently a professor in the Department of Computer Science and Electrical Engineering. He was a

visiting research specialist in the Institute of Information Engineering at the National Cheng Kung University, Tainan, Taiwan, in 1994–1995. He received a National Research Council senior research associateship award in 2002–2003, sponsored by the U.S. Army Soldier and Biological Chemical Command, Edgewood Chemical and Biological Center, Aberdeen Proving Ground, Maryland. He is currently a distinguished lecture chair at the National Chung Hsing University sponsored by the Ministry of Education, Taiwan, ROC from 2005–2006 and is currently holding a Chair Professorship with the Environmental Restoration and Disaster Reduction Center and Department of Electrical Engineering, National Chung Hsing University, Taichung, Taiwan, ROC. He has three patents and several pending on hyperspectral image processing. He was on the editorial board of the *Journal of High Speed Networks* and was the guest editor of a special issue of the same journal on telemedicine and applications (April, 2000) and also co-guest editor of a special issue on Broadband Multimedia Sensor Networks in Healthcare Applications (April, 2007). He is also a co-guest editor of a special issue on High Performance Computing Hyperspectral Imaging for *International Jour-*

nal of High Performance Computing Applications (December 2007). His research interests include multispectral and hyperspectral image processing, automatic target recognition, medical imaging, information theory and coding, signal detection and estimation, and neural networks. He has authored a book, *Hyperspectral Imaging: Techniques for Spectral Detection and Classification*, published by Kluwer Academic Publishers in 2003 and edited two books, *Recent Advances in Hyperspectral Signal and Image Processing*, Trivandrum, Kerala: Research Signpost, Trasworld Research Network, India, 2006 and *Hyperspectral Data Exploitation: Theory and Applications*, John Wiley & Sons, 2007. He is currently working on his second book, *Hyperspectral Imaging: Signal Processing Algorithm Design and Analysis*, John Wiley & Sons, 2007 and co-edit with A. Plaza a book on *High Performance Computing in Remote Sensing*, CRC Press, 2007. Dr. Chang is an associate editor in the area of hyperspectral signal processing for *IEEE Transactions on Geoscience and Remote Sensing*, 2001–2007, a fellow of SPIE, and a member of Phi Kappa Phi and Eta Kappa Nu.